CCS Chemistry

COMMUNICATION

Received: Feb. 28, 2022 | Accepted: Apr. 10, 2022 | Published: May 27, 2022

Efficient Photocatalytic Reduction of CO_2 Catalyzed by the Metal–Organic Framework MFM-300(Ga)

Tian Luo[1], Zi Wang[1,2], Xue Han[1], Yinlin Chen[1], Dinu Iuga[3], Daniel Lee[4], Bing An[1], Shaojun Xu[1], Xinchen Kang[5], Floriana Tuna[1,2], Eric J. L. McInnes[1,2], Lewis Hughes[6], Ben F. Spencer[7], Martin Schröder[1]* & Sihai Yang[1]*

[1]Department of Chemistry, University of Manchester, Manchester M13 9PL, [2]Photon Science Institute (PSI), University of Manchester, Manchester M13 9PL, [3]Department of Physics, University of Warwick, Coventry CV4 7AL, [4]Department of Chemical Engineering and Analytical Science, University of Manchester, Manchester M13 9PL, [5]Institute of Chemistry, Chinese Academy of Science, Beijing 100190, [6]Department of Earth and Environmental Sciences, University of Manchester, Manchester M13 9PL, [7]Department of Materials, University of Manchester, Manchester M13 9PL

*Corresponding authors: M.Schroder@manchester.ac.uk; Sihai.Yang@manchester.ac.uk

Cite this: *CCS Chem.* **2022**, 4, 2560–2569
DOI: 10.31635/ccschem.022.202201931

Photocatalytic reduction of CO_2 to carbon fuels is an important target but highly challenging to achieve. Here, we report the efficient photoconversion of CO_2 into formic acid over a Ga(III)-based metal–organic framework (MFM) material using triethanolamine as the sacrificial agent. Under light irradiation and at room temperature, photoreduction of CO_2 over MFM-300(Ga) yields formic acid with a selectivity of 100%, a high productivity of 502 ± 18 μmol·g_{cat}^{-1}·h^{-1}, and excellent catalytic stability. In situ electron paramagnetic resonance spectroscopy reveals that MFM-300(Ga) promotes the generation of $CO_2^{\bullet-}$ radical anions as a reaction intermediate driven by strong binding and activation of CO_2 molecules at the bridging –OH sites within the pore. This study represents the first example of a Ga(III)-based MOF catalyst for CO_2 reduction.

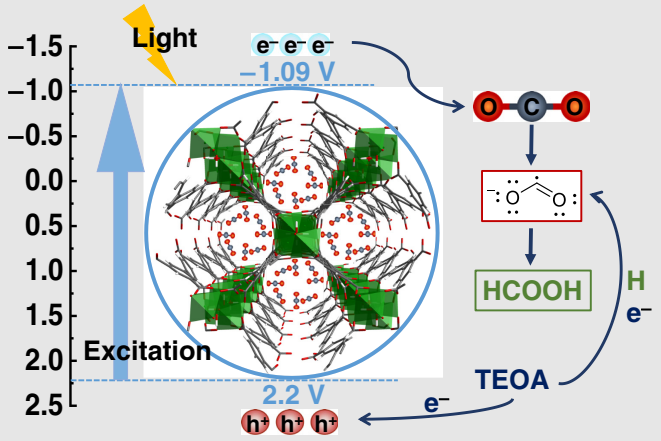

Keywords: **MFM-300, metal–organic framework, CO_2 reduction, photocatalysis, host–guest interaction**

Introduction

The development of efficient photocatalysts to convert CO_2 into value-added chemicals has attracted much interest.[1,2] In addition to TiO_2, various Ga-based semiconductors, such as GaN, GaP, Ga_2O_3, and $ZnGa_2O_4$, have been widely investigated as photocatalysts to drive this reaction.[3–7] However, their wide optical bandgap (E_g) restricts the use of solar light mainly to the ultraviolet region, and, more importantly, their nonporous nature limits the mass transport of CO_2. This impedes charge transfer between catalyst and substrate and also leads to the undesirable recombination of photogenerated electrons and holes.[8] A number of strategies have been exploited to improve the photocatalytic performance of Ga-based semiconductors. For example, doping of metals (e.g., Ge, Zn) or nonmetals (e.g., N, Si) can narrow the bandgap and improve the light-harvesting efficiency

DOI: 10.31635/ccschem.022.202201931
Citation: *CCS Chem.* **2022**, 4, 2560–2569
Link to VoR: https://doi.org/10.31635/ccschem.022.202201931

of the resultant material.[9-12] Fabrication of ultrathin nanosheets, nanowires, or porous structures can increase the surface area and CO_2 uptake.[13-15] Meanwhile the introduction of a cocatalyst, noble metal nanoparticles, or a second semiconductor to construct *Z*-scheme or heterojunction-type systems can promote electron transfer.[10,16-18] However, the photocatalytic efficiency over state-of-the-art Ga-based semiconductors remains limited, and only gaseous products such as CH_4 and CO are produced. For example, a top-performing heterostructure of Au/Al_2O_3/p-GaN shows a photocatalytic productivity for CO of 230 $\mu mol \cdot g^{-1} \cdot h^{-1}$.[4]

Metal–organic framework (MOF) materials incorporate active sites fixed uniformly in 3D space, thus preventing aggregation of catalytic centers and potentially enhancing charge separation. MOFs are therefore emerging as important photocatalysts for the reduction of CO_2, showing potential to overcome the barriers of conventional semiconductors.[19,20] For example, the intrinsic microporosity and catalytically active sites confined in MOFs can form unique "microreactors" to promote the adsorption and activation of CO_2 via the formation of strong host–guest interactions.[21] More importantly, the backbone of MOFs consisting of infinite metal-ligand linkages

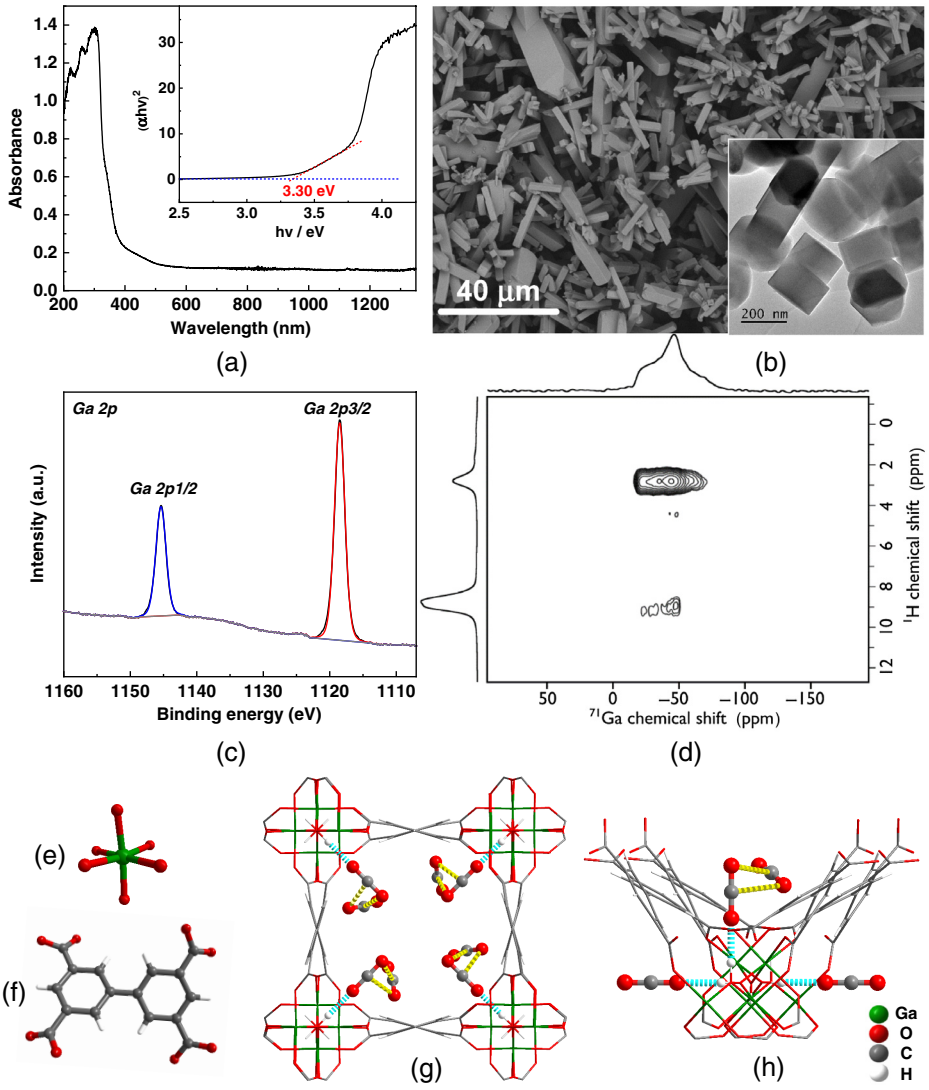

Figure 1 | *Characterisation and crystal structure of MFM-300(Ga). (a) The UV-DRS spectrum of MFM-300(Ga) with Tauc plot (insert); (b) SEM image of MFM-300(Ga) with TEM image (insert); (c) high-resolution XPS spectrum of Ga 2p, and (d) ^{71}Ga{1H} D-HMQC 2D MAS NMR spectrum of MFM-300(Ga) and corresponding 1D direct excitation ^{71}Ga (top) and ^{1}H (left) MAS NMR spectra, recorded at 20.0 T with a MAS frequency of 60 kHz; crystal structure of MFM-300 (Ga): (e) octahedral [$GaO_4(OH)_2$]; (f) ligand; (g and h) views of binding sites (bridging –OH groups) for adsorbed CO_2 molecules within MFM-300(Ga) studied by In situ synchrotron X-ray single-crystal diffraction.[25] Host–guest hydrogen bonds and intermolecular dipole interactions are highlighted in cyan and yellow, respectively.*

DOI: 10.31635/ccschem.022.202201931
Citation: *CCS Chem.* **2022**, 4, 2560–2569
Link to VoR: https://doi.org/10.31635/ccschem.022.202201931

can facilitate efficient ligand-to-metal-charge-transfer (LMCT), thus prolonging the excitation lifetime by boosting the isolation and utilisation of photoinduced electrons.[22] A number of MOF systems have been tested for photoreduction of CO_2,[19,20] and Ti-based MOFs are particularly attractive.[23,24] In contrast, to date, no Ga-based MOF has been shown to exhibit activity for CO_2 conversion, and we report here the first example for the efficient photoreduction of CO_2. Under light irradiation and at room temperature, MFM-300(Ga) catalyzes the conversion of CO_2 into formic acid with a 100% selectivity and an excellent productivity up to 502 ± 18 $\mu mol \cdot g_{cat}^{-1} \cdot h^{-1}$, significantly higher than conventional Ga-based semiconductors and among the best-behaving MOF-based photocatalysts for this reaction. Importantly, in situ electron paramagnetic resonance (EPR) spectroscopy confirms that the CO_2 radical anion ($CO_2^{\bullet-}$) is generated as an intermediate to the production of formic acid over MFM-300(Ga).

Results and Discussion

MFM-300(Ga), $[Ga_2(OH)_2(L)]$ (H_4L = biphenyl-3,3′,5,5′-tetracarboxylic acid) was chosen for the photoreduction of CO_2 due to its high stability, high adsorption, and strong binding of CO_2 molecules via the formation of hydrogen bonds to the bridging –OH groups in the pore.[25] MFM-300(Ga) is comprised of chains of $[GaO_4(OH)_2]_\infty$ octahedra linked by *cis*-μ_2-OH groups, and these chains are further bridged by tetracarboxylate ligands to form a 'wine rack' open framework. Desolvated MFM-300(Ga) shows a Brunauer–Emmett–Teller (BET) surface area of 1064 $m^2 \cdot g^{-1}$ and an uptake of CO_2 of 5.00 $mmol \cdot g^{-1}$ at 298 K and 1 bar (see Supporting Information Figure S1). The purity of the bulk material has been confirmed by powder X-ray diffraction (PXRD) (see Supporting Information Figure S2) and thermogravimetric analysis (see Supporting Information Figure S3a). Scanning electron microscopy (SEM) and transmission electron microscopy (TEM) show that crystals of MFM-300(Ga) exhibit cuboid-shaped morphology with an average size of 15 μm (Figure 1b). High-resolution X-ray photoelectron spectroscopy (XPS) analysis of MFM-300(Ga) shows the peaks of Ga $2p_{1/2}$, $2p_{3/2}$, $3d_{3/2}$, and $3d_{5/2}$ at 1145.5, 1118.6, 21.2, and 20.7 eV, respectively, consistent with the trivalent Ga(III) (Figure 1c, see Supporting Information Figure S4). Solid-state ^{13}C and ^{71}Ga NMR spectroscopy reveal a highly ordered structure consistent with a single repeating octahedral $[GaO_4(OH)_2]$ environment (see Supporting Information Figure S5).[26] The high-field $^{71}Ga\{^1H\}$ 2D through-space (dipolar) heteronuclear correlation NMR spectrum of MFM-300(Ga) demonstrates this more extensively with strong correlations between the Ga environment and the hydroxyls (at $\delta\{^1H\}$ = 2.8 ppm) and a weaker interaction with the more distant aromatic proton between the carboxylates (at $\delta\{^1H\}$ = 9.0 ppm), with no other correlations observed (Figure 1d). Moreover, the ratio of the ^1H NMR signal intensities of the aromatic protons to the hydroxy protons is ~3:1 (see Supporting Information Figure S5c), entirely consistent with the structural model shown in Figures 1e–1h. Solid-state UV–vis diffuse reflectance spectroscopy (UV-DRS) of MFM-300(Ga) shows an intensive and broad absorption band in the ultraviolet region, which is assigned to the π→π* transition of the biphenyl ligand (Figure 1a).[27] The Tauc plot yields an optical bandgap of 3.30 eV, lower than that of commercial Ga_2O_3 (E_g = 4.56, 4.70, and 4.67 eV for α-, β-, and γ-Ga_2O_3, respectively)[28] and $ZnGa_2O_4$ (E_g = 4.18 eV).[9] The photocurrent response of MFM-300(Ga) confirms that the current density increases upon irradiation and decreases upon turning off the light (see Supporting Information Figure S6).

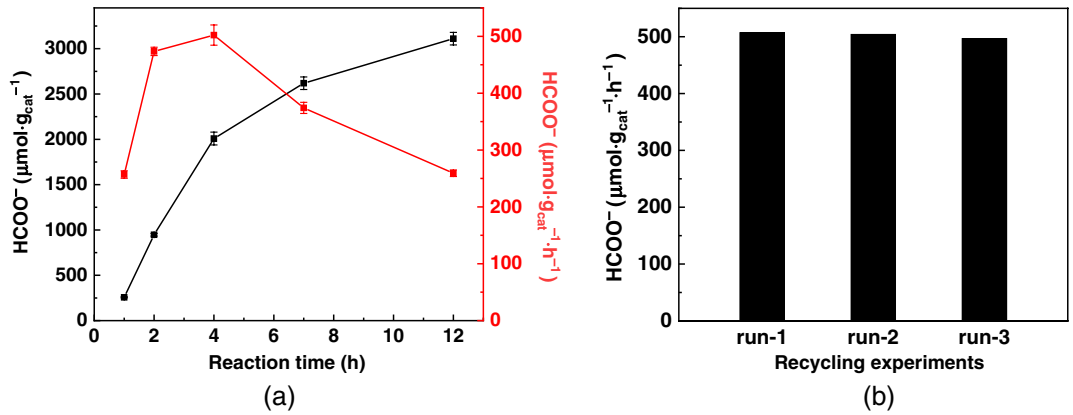

Figure 2 | *Photocatalytic CO_2 reduction over MFM-300(Ga). (a) Different reaction time; (b) recycling tests. Reaction conditions: MFM-300(Ga) (10 mg), TEOA/CH_3CN (3 mL/15 mL, saturated with CO_2), 25 °C, 350–780 nm, light irradiation for 4 h.*

DOI: 10.31635/ccschem.022.202201931
Citation: *CCS Chem.* **2022**, 4, 2560–2569
Link to VoR: https://doi.org/10.31635/ccschem.022.202201931

The photocatalytic activity of MFM-300(Ga) toward the reduction of CO_2 has been studied in CO_2-saturated CH_3CN-containing triethanolamine (TEOA) as the sacrificial agent under irradiation at 350–780 nm for 1–12 h. The gaseous products were analysed by gas chromatography and the liquid product by ^1H NMR spectroscopy. The photocatalytic efficiency was measured as the moles of product obtained per gram of catalyst per hour ($mol{\cdot}g_{cat}^{-1}{\cdot}h^{-1}$) to afford a direct comparison with reported catalysts. Formic acid was the only product detected in the liquid phase, and no carbon-containing gaseous products were detected. The photocatalytic performance as a function of reaction time over MFM-300(Ga) indicates that a high productivity of 502 ± 18 $\mu mol{\cdot}g_{cat}^{-1}{\cdot}h^{-1}$ for formic acid was achieved at 4 h (Figures 2a, see Supporting Information Figure S7). More importantly, the photocatalytic activity and the crystallinity of MFM-300(Ga) were retained over three cycles of reaction (Figure 2b). The photocatalytic efficiency of MFM-300(Ga) is higher than the majority of reported MOFs (Table 1) for converting CO_2 into formic acid, such as amino-functionalised MIL-125(Ti), UiO-66(Zr), and MIL-101(Fe),[23,31,44] and is only lower than two cases. One is the mixed metal and mixed ligand systems of NH_2-UiO-66(Zr/Ti) and $(NH_2)_2$-UiO-66(Zr/Ti),[24] which are prepared via post-synthetic modifications to introduce Ti(IV) sites into the framework. The other is a recent report describing a π-conjugated naphthoporphyrin system constructed with Zr metal clusters, which demonstrates the highest value (6630 $\mu mol{\cdot}g_{cat}^{-1}{\cdot}h^{-1}$) reported in the literature.[29] A comparison of state-of-the-art studies of thermal hydrogenation of CO_2 into formic acid over MOF-based catalysts is given in Supporting Information Table S1.

To gain further insights into this reaction, a series of control experiments were conducted (Table 2). No carbon-containing product was detected from reactions in the absence of (1) MFM-300(Ga), (2) CO_2 (where N_2 is used instead), or (3) light. These results confirm that the carbon source of formic acid is CO_2 and that the reaction proceeds via photocatalytic routes driven by the MOF catalyst. Replacement of TEOA with triethylamine (TEA)[45] gives a low productivity of 64 $\mu mol{\cdot}g_{cat}^{-1}{\cdot}h^{-1}$ for formic acid, which is consistent with recent reports on the important role of TEOA in binding and assisting the transport of CO_2 in CH_3CN.[46,47] A range of different organic solvents have been tested, and CH_3CN demonstrates the highest activity due to the optimal efficiency of mass transfer and the enhanced binding of CO_2 by TEOA in CH_3CN[47] (see Supporting Information Figure S8). Interestingly, no product was observed when using Ga_2O_3 (~50 mesh, E_g = 4.57), GaN (E_g = 3.04), GaP (E_g = 1.92), or a powdered mixture of $Ga(NO_3)_3$ and H_4L as the photocatalyst (see Supporting Information Figure S9). This indicates that the

Table 1 | *Comparison of the Photocatalytic Efficiency of MFM-300(Ga) and a Selection of MOFs Reported for this Reaction in the Literature*

MOF-Based Materials	Chemical Formula	CO_2 Uptake /$mmol{\cdot}g^{-1}$ (1 atm)	Sacrificial Agent	Solvents	Photocatalytic Efficiency ($\mu mol{\cdot}g_{cat}^{-1}{\cdot}h^{-1}$)	References
TNP-MOF	$Zr_6(OH)_4O_4(TNP)_3$	1.69 (273 K) 1.03 (298 K)	TEOA	CH_3CN	6630	29
NH_2-UiO-66-Zr(Ti) $(NH_2)_2$-UiO-66-Zr(Ti)	- $Zr_{4.3}Ti_{1.7}O_4(OH)_4(C_8H_7O_4N)_{5.17}(C_8H_8O_4N_2)_{0.83}$	-	TEOA and BNAH	CH_3CN	782 1052	24
MFM-300(Ga)	$Ga_2(OH)_2(L)$	6.77 (273 K) 5.00 (298 K)	TEOA	CH_3CN	502	This work
Co-MOF, LIFM-45	$Co_3(HL^O)_2{\cdot}4DMF{\cdot}4H_2O$	-	BNAH	DMAc	456	30
NH_2-MIL-101(Fe)	$Fe_3OCl(H_2O)_3(BDC\text{-}NH_2)_3$	1.52 (273 K)	TEOA	CH_3CN	445	31
MIL-101(Fe)	$Fe_3OCl(H_2O)_3(BDC)_3$	1.18 (273 K)			148	
NH_2-MIL-53(Fe)	$Fe^{III}(OH)(BDC\text{-}NH_2)$	0.89 (273 K)			116	
MIL-53(Fe)	$Fe^{III}(OH)(BDC)$	0.60 (273 K)			74	
NH_2-MIL-88(Fe)	$Fe^{III}_3O(CH_3OH)_3(BDC\text{-}NH_2)_3$	0.64 (273 K)			75	
MIL-88(Fe)	$Fe^{III}_3O(CH_3OH)_3(BDC)_3$	0.46 (273 K)			23	

(Continues)

DOI: 10.31635/ccschem.022.202201931
Citation: *CCS Chem.* **2022**, 4, 2560–2569
Link to VoR: https://doi.org/10.31635/ccschem.022.202201931

DOI: 10.31635/ccschem.022.202201931
Citation: CCS Chem. 2022, 4, 2560–2569
Link to VoR: https://doi.org/10.31635/ccschem.022.202201931

TABLE 1 *(Continued)*

MOF-Based Materials	Chemical Formula	CO_2 Uptake /mmol·g^{-1} (1 atm)	Sacrificial Agent	Solvents	Photocatalytic Efficiency (μmol·g_{cat}^{-1}·h^{-1})	References
AD-MOF-2	$[Co_2(HAD)_2(AD)_2\ (IA)_2]$·DMF	1.86 (298 K)	TIPA	CH_3CN	443	32
AD-MOF-1	$[Co_2(HAD)_2\ (AD)_2$-(BA)]·DMF·$2H_2O$	2.33 (298 K)			179	
Fe_3-Fe_2-NH_2	[{Fe_2-Tri}{$Fe_3(\mu_3$-O)(BDC-$NH_2)_3$}]·$4NO_3$	1.38 (298 K)	TIPA	CH_3CN/H_2O	396	33
Fe_3-Fe_2	[{Fe_2-Tri}{$Fe_3(\mu_3$-O)$(BDC)_3$}]·$4NO_3$	1.23 (298 K)		(1:1)	309	
PCN-138	$[Zr_6(\mu_3\text{-}O)_4(\mu_3\text{-}OH)_4]$[TCPP][$TBTB]_{8/3}$	2.82 (273 K)	TIPA	H_2O	168	34
		1.82 (298 K)				
Ir-CP	[Y(Ir(ppy)$_2$(dcbpy)$_2$][OH]	–	TEOA	CH_3CN	158	35
Eu-Ru(Phen)$_3$	$[Eu_2(\mu_2\text{-}H_2O)(H_2O)_3(L^1)_2]$·$(NO_3)_2$·(2-FBA)$_2$·$(H_2O)_{22}$	–	TEOA	CH_3CN	94	36
Cd/Ru-MOF-1	{Cd_3[Ru-L^2]$_2$·2(Me_2NH_2)·solvent}n	–	TEOA	CH_3CN	67	37
Cd/Ru-MOF-2	{Cd[Ru-L^3]·3(H_2O)}n				72	
PCN-222(Zr)	$Zr_6(\mu_3\text{-}OH)_8(OH)_8(TCPP)_2$	2.59 (273 K)	TEOA	CH_3CN	60	38
		1.56 (298 K)				
NNU-28(Zr)	$[Zr_6O_4(OH)_4(L^4)_6]$·6DMF	2.83 (273 K)	TEOA	CH_3CN	53	39
		1.49 (298 K)				
PCN-136	$Zr_6(\mu_3\text{-}O)4(\mu_3\text{-}OH)_4(OH)_6(H_2O)_6$(HCHC)	2.72 (273 K)	TIPA	CH_3CN/H_2O	44	40
Zr-SDCA-NH_2	$[Zr_6O_4(OH)_4(L^5)_6]$·8DMF	3.74 (273 K)	TEOA	CH_3CN	41	41
		1.57 (298 K)				
NNU-31-Zn	$Fe_2Zn(\mu_3\text{-}O)(TCA)_2(H_2O)_3$	1.65 (298 K)	–	H_2O	26	42
NH_2-MIL-125(Ti)	$Ti_8O_8(OH)_4$(BDC-$NH_2)_6$	5.90 (273 K)	TEOA	CH_3CN	16	23
MIL-125(Ti)	$Ti_8O_8(OH)_4(BDC)_6$	4.40 (273 K)			4	
NH_2-UiO-66-(Zr/Ti)	(Zr/Ti)$_6O_4(OH)_4$(BDC-$NH_2)_6$	3.79 (273 K)	TEOA	CH_3CN	12	43
NH_2-UiO-66(Zr)	$Zr_6O_4(OH)_4$(BDC-$NH_2)_6$	3.04 (273 K)			7	
NH_2-UiO-66(Zr)	$Zr_6O_4(OH)_4$(BDC-$NH_2)_6$	3.04 (273 K)	TEOA	CH_3CN	26	44
UiO-66(Zr)	$Zr_6O_4(OH)_4(BDC)_6$	2.37 (273 K)			0	

Notes: TEOA, triethanolamine; BNAH, 1-benzyl-1,4-dihydronicotinamide; H_4L, biphenyl-3,3′,5,5′-tetracarboxylic acid; H_2BDC, benzene-1,4-dicarboxylic acid; HAD, adenine; BA, butanedioic acid; IA, isobutyric acid; DMF, *N*,*N*-dimethylformamide; Tri, 1,2,4-triazole; DMAc, *N*,*N*-dimethylacetamide; TIPA, triisopropanolamine; H_2TCPP, tetrakis(4-carboxyphenyl)porphyrin; TBTB, 4,4′,4″-(2,4,6-trimethylbenzene-1,3,5-triyl)tribenzoate; ppy, 2-phenylpyridine; dcbpy, 2,2′-bipyridine-4,4′-dicarboxylate; H_4L^0, 2′-amino-[1,1′:4′,1″-terphenyl]-3,3″,5,5″-tetracarboxylic acid; H_3L^1, Ru(phen)3-derived tricarboxylate acid metalloligand; 2-FBA, 2-fluorobenzoate; L^2=5,5′-dcbpy=2,2′-bipyridine-5,5′-dicarboxylate; L^3=(4,4′-dcbpy)2(bpy), bpy=2,2′-bipyridine; H_2L^4, 4,4′-(anthracene-9,10-diylbis(e-thyne-2,1-diyl))dibenzoic acid; HCHC, hexakis(4-carboxyphenyl)hexabenzocoronene; H_2L^5, 2,2′-diamino-4,4′-stilbene dicarboxylic acid; TCA, 4,4′,4″-tricarboxytriphenylamine.

Table 2 | *Summary of Reaction Conditions of Comparison Experiments*

Entry	Catalyst	Light (nm)		Gas	HCOOH
1	MFM-300(Ga)	350–780	TEOA	CO_2	502
2	n.a.	350–780	TEOA	CO_2	n.a.
3	MFM-300(Ga)	350–780	TEOA	N_2	n.a.
4	MFM-300(Ga)	350–780	n.a.	CO_2	n.a.
5	MFM-300(Ga)	n.a.	TEOA	CO_2	n.a.
6	MFM-300(Ga)	350–780	TEA	CO_2	64
7	$Ga(NO_3)_3{\cdot}9H_2O$ and H_4L	350–780	TEOA	CO_2	n.a.
8	Ga_2O_3	350–780	TEOA	CO_2	n.a.
9	GaN	350–780	TEOA	CO_2	n.a.
10	GaP	350–780	TEOA	CO_2	n.a.
11	MIL-53(Ga)	350–780	TEOA	CO_2	n.a.
12	MIL-68(Ga)	350–780	TEOA	CO_2	n.a.

Reaction conditions: MFM-300(Ga) (10 mg), TEOA/CH_3CN (3 mL/15 mL, saturated with CO_2), 25 °C, 350–780 nm, light irradiation for 4 h. For entry 6, 3 mL TEA was added to replace TEOA; For entry 7, a powdered mixture of $Ga(NO_3)_3{\cdot}9H_2O$ (0.04 mmol, 16.7 mg) and H_4L (0.02 mmol, 6.6 mg) were used (H_4L, biphenyl-3,3,5′,5′-tetracarboxylic acid); For entry 8–12, the catalysts used were 10 mg in each reaction.

framework structure of MFM-300(Ga) is crucial for adsorption of CO_2 and the separation and transfer of photoinduced electrons.

To investigate the effects of ligands and framework structures of Ga-MOFs on the photocatalytic property, MIL-53(Ga) and MIL-68(Ga), both constructed from terephthalic acid, were studied for this reaction.[48–50] The phase purity of these MOFs has been confirmed by PXRD (see Supporting Information Figure S10). The bandgaps for MIL-53(Ga) and MIL-68(Ga) are determined to be 3.21 and 3.93 eV, respectively, by UV-DRS analysis (see Supporting Information Figure S11). Under the same reaction conditions as above, neither MOF shows photocatalytic activity toward the reduction of CO_2. Although showing similar BET surface areas (1117–1140 $m^2{\cdot}g^{-1}$) and a structure comprising $[GaO_4(OH)_2]$ moieties, the CO_2 adsorption capacity of MIL-53(Ga) and MIL-68(Ga) (1.46–1.65 $mmol{\cdot}g^{-1}$) is much lower than that (5.00 $mmol{\cdot}g^{-1}$) of MFM-300(Ga) (see Supporting Information Table S2). This is likely due to the rigid framework and presence of active μ_2-OH sites in MFM-300(Ga) that promote the transport and binding of CO_2 as confirmed by in situ crystallographic and spectroscopic analyses.[25] Furthermore, the biphenyl ligand of MFM-300(Ga) demonstrates increased π-electron delocalisation in the framework backbone and hence enhanced LMCT compared with terephthalate in MIL-53(Ga) and MIL-68(Ga). These collectively result in the drastic difference in their photocatalytic activity.

Photophysical and electrochemical experiments were conducted to understand the redox properties of MFM-300(Ga). Mott-Schottky (MS) analysis and valence-band XPS studies were conducted to determine the positions of the conduction band (E_{CB}) and the valence band (E_{VB}) of MFM-300(Ga), respectively.[32,51] The E_{VB} is determined to be 2.2 V versus normalised hydrogen electrode (NHE) from the VB-XPS result (see Supporting Information Figure S12a). The positive slope of all MS plots recorded at different frequencies indicates that MFM-300(Ga) is a typical *n*-type semiconductor, and the intercept is independent of the frequency. The flat band potential (E_{FB}) is determined as –0.99 V versus NHE (see Supporting Information Figure S12b), which is usually ~0.1 V more positive than the E_{CB} for *n*-type materials.[52] Thus, the E_{CB} is estimated to be –1.09 V versus NHE. The gap between VB and CB is thus 3.29 eV, which is in excellent agreement with the bandgap of 3.30 eV obtained from UV-DRS analysis.

To identify the radical species involved in the catalytic process, in situ spin-trapping EPR experiments under photocatalytic conditions were conducted. Since the lifetime of free radicals is several orders of magnitude shorter than the acquisition time of EPR spectra, 5,5-dimethyl-1-pyrroline-n-oxide (DMPO) was used as a spin trap to enable the identification of radicals as long-lived DMPO-radical adducts.[53] An intense six-line signal with g = 2.005 and hyperfine coupling constants A^N = 15.2 G and A^H = 18.9 G was detected and unambiguously assigned to DMPO-$CO_2^{\bullet-}$[54,55] (see Figure 3a and Supporting Information Table S3). This indicates that the CO_2 radical anion ($CO_2^{\bullet-}$) is the direct intermediate to form formic acid. No radical was captured for the reaction conducted under dark conditions. Significantly, to the best of our knowledge, this is the first time that a direct intermediate radical has been detected in the photoreduction of CO_2 over a MOF-based catalyst.

The catalytic cycle for this reaction is proposed (Figure 3b). Upon light irradiation, MFM-300(Ga) is activated, and the electrons in the VB (2.2 V) are promoted to the CB (–1.09 V), and the photoinduced holes at the VB are readily filled up by the electron sacrificial agent TEOA. Surprisingly, the photoinduced electrons with a reductive potential of –1.09 V versus NHE can reduce CO_2 to $CO_2^{\bullet-}$ radical anions, given the strongly negative redox potential of –1.90 V versus NHE [Eq. (1)] for this process.[56] This indicates that the strong binding of CO_2 molecules to the bridging μ_2-OH sites of MFM-300(Ga) through the formation of hydrogen bonds as determined by in situ synchrotron X-ray diffraction[25] not only promotes the transfer of photoinduced electrons from MFM-300(Ga) to the bound CO_2 molecules but also activates the adsorbed CO_2 molecules. This shifts the reduction to a more anodic potential. Interestingly, the path of photocatalytic reduction of CO_2 into formic acid is widely regarded as accepting electrons and protons

DOI: 10.31635/ccschem.022.202201931
Citation: *CCS Chem.* **2022**, 4, 2560–2569
Link to VoR: https://doi.org/10.31635/ccschem.022.202201931

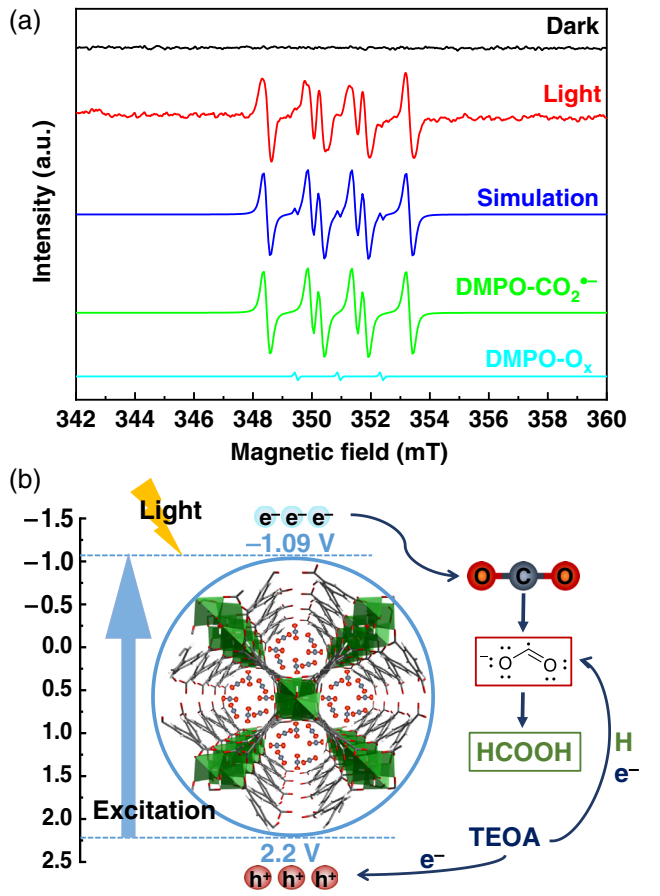

Figure 3 | *(a) In situ X-band EPR spectra of photocatalytic reactions over MFM-300(Ga) using DMPO as spin trap, (black) before and (red) after light irradiation, with simulated (blue) spectrum showing a major component, DMPO-$CO_2^{\bullet-}$ (green, simulation), and a minor component, DMPO-O_x (cyan, simulation) under photocatalytic conditions over MFM-300(Ga). (b) The proposed mechanism of the photocatalytic reduction of CO_2 over MFM-300(Ga).*

simultaneously at a redox potential of −0.61 V versus NHE [Eq. (2)].[56] By contrast, the adsorbed CO_2 molecule in MFM-300(Ga) is able to accept a single electron via host–guest hydrogen bonding to generate a $CO_2^{\bullet-}$ radical anion, which is unprecedented in the MOF-driven photoreduction of CO_2 and affords new insights into the mechanism of photocatalytic reduction of CO_2. Recently, the positive impact of strong host-guest interactions on the activation of the adsorbed substrate has also been demonstrated by the conversion of small molecules over porous catalysts.[57,58] Thus, the photocatalytic activity of MOFs is determined by the synergistic effect of bandgap, rate of charge transfer, uptake of CO_2, and most importantly, the interaction between the catalyst scaffold and adsorbed CO_2 molecules, which will inform the design of new photocatalysts.

$$CO_2 + e^- \rightarrow CO_2^{\bullet-} \qquad E^0_{redox} = -1.90 \text{ V vs. NHE} \qquad (1)$$

$$CO_2 + 2H^+ + 2e^- + HCOOH \qquad E^0_{redox} = -0.61 \text{ V vs. NHE} \qquad (2)$$

Conclusion

The porosity and design flexibility of MOFs, coupled with their intrinsic semiconductor and photoelectrical properties, make them promising candidates as efficient photocatalysts. We report the first example of a Ga-MOF-based semiconductor that can promote the photoreduction of CO_2 to formic acid with a selectivity of 100% and a high productivity of 502 ± 18 $\mu mol \cdot g_{cat}^{-1} \cdot h^{-1}$ under light irradiation and at room temperature using TEOA as an electron sacrificial agent. MFM-300(Ga) shows excellent catalytic stability over three cycles of reactions with full retention of the productivity of formic acid. In situ EPR spectroscopic analysis confirms the generation of the $CO_2^{\bullet-}$ radical anion as the reaction intermediate promoted by the strong host–guest interactions between the bridging μ_2-OH groups of MFM-300(Ga) and the adsorbed CO_2 molecules. Compared with other reported Ga-MOFs in literature, the presence of strong binding sites and efficient LMCT plays an important role in boosting the photocatalytic activity toward CO_2 reduction, which sheds light on the design of future MOF-based photocatalysts with improved activity.

Supporting Information

Supporting Information is available and includes detailed experimental procedures and characterization data.

Conflict of Interest

There is no conflict of interest to report.

Acknowledgments

This research was supported by EPSRC (EP/I011870, EP/V056409), the Royal Society and the University of Manchester with funding, and EPSRC for funding of the EPSRC National EPR Facility at the University of Manchester. This project has also received funding from the European Research Council under the European Union's Horizon 2020 research and innovation programme (grant agreement No 742401, NANOCHEM). The UK High-Field Solid-State NMR Facility used in this research was funded by EPSRC and BBSRC (EP/T015063/1) as well as the University of Warwick including via partial funding through Birmingham Science City Advanced Materials Projects 1 and 2 supported by Advantage West Midlands and the European Regional Development Fund.

DOI: 10.31635/ccschem.022.202201931
Citation: *CCS Chem.* **2022**, 4, 2560–2569
Link to VoR: https://doi.org/10.31635/ccschem.022.202201931

The authors wish to acknowledge Dr. Marek Nikiel for the help with XPS measurement.

References

1. Ran, J.; Jaroniec, M.; Qiao, S. Z. Cocatalysts in Semiconductor-Based Photocatalytic CO_2 Reduction: Achievements, Challenges, and Opportunities. *Adv. Mater.* **2018**, *30*, 1704649.
2. Zhang, W.; Mohamed, A. R.; Ong, W. J. Z-Scheme Photocatalytic Systems for Carbon Dioxide Reduction:Where Are We Now? *Angew. Chem. Int. Ed.* **2020**, *59*, 22894–22915.
3. Dhakshinamoorthy, A.; Navalon, S.; Corma, A.; Garcia, H. Photocatalytic CO_2 Reduction by TiO_2 and Related Titanium Containing Solids. *Energy Environ. Sci.* **2012**, *5*, 9217–9233.
4. Li, R.; Cheng, W.-H.; Richter, M. H.; DuChene, J. S.; Tian, W.; Li, C.; Atwater, H. A. Unassisted Highly Selective Gas-Phase CO_2 Reduction with a Plasmonic Au/p-GaN Photocatalyst Using H_2O as an Electron Donor. *ACS Energy Lett.* **2021**, *6*, 1849–1856.
5. Barton, E. E.; Rampulla, D. M.; Bocarsly, A. B. Selective Solar-Driven Reduction of CO_2 to Methanol Using a Catalyzed p-GaP Based Photoelectrochemical Cell. *J. Am. Chem. Soc.* **2008**, *130*, 6342–6344.
6. Akatsuka, M.; Kawaguchi, Y.; Itoh, R.; Ozawa, A.; Yamamoto, M.; Tanabe, T.; Yoshida, T. Preparation of Ga_2O_3 Photocatalyst Highly Active for CO_2 Reduction with Water Without Cocatalyst. *Appl. Catal. B Environ.* **2020**, *262*, 118247.
7. Yan, S. C.; Ouyang, S. X.; Gao, J.; Yang, M.; Feng, J. Y.; Fan, X. X.; Wan, L. J.; Li, Z. S.; Ye, J. H.; Zhou, Y.; Zou, Z. G. A Room-Temperature Reactive-Template Route to Mesoporous $ZnGa_2O_4$ with Improved Photocatalytic Activity in Reduction of CO_2. *Angew. Chem. Int. Ed.* **2010**, *122*, 6544–6548.
8. Marszewski, M.; Cao, S.; Yu, J.; Jaroniec, M. Semiconductor-Based Photocatalytic CO_2 Conversion. *Mater. Horizons* **2015**, *2*, 261–278.
9. Yan, S.; Wang, J.; Gao, H.; Wang, N.; Yu, H.; Li, Z.; Zhou, Y.; Zou, Z. Zinc Gallogermanate Solid Solution: A Novel Photocatalyst for Efficiently Converting CO_2 into Solar Fuels. *Adv. Funct. Mater.* **2013**, *23*, 1839–1845.
10. Tatsumi, H.; Teramura, K.; Huang, Z.; Wang, Z.; Asakura, H.; Hosokawa, S.; Tanaka, T. Enhancement of CO Evolution by Modification of Ga_2O_3 with Rare-Earth Elements for the Photocatalytic Conversion of CO_2 by H_2O. *Langmuir* **2017**, *33*, 13929–13935.
11. Yan, S.; Yu, H.; Wang, N.; Li, Z.; Zou, Z. Efficient Conversion of CO_2 and H_2O into Hydrocarbon Fuel over $ZnAl_2O_4$-Modified Mesoporous ZnGaNO under Visible Light Irradiation. *Chem. Commun.* **2012**, *48*, 1048–1050.
12. Sekimoto, T.; Hashiba, H.; Shinagawa, S.; Uetake, Y.; Deguchi, M.; Yotsuhashi, S.; Ohkawa, K. Analysis of Products from Photoelectrochemical Reduction of $^{13}CO_2$ by GaN-Si Based Tandem Photoelectrode. *J. Phys. Chem. C* **2016**, *120*, 13970–13975.
13. Liu, Q.; Wu, D.; Zhou, Y.; Su, H.; Wang, R.; Zhang, C.; Yan, S.; Xiao, M.; Zou, Z. Single-Crystalline, Ultrathin $ZnGa_2O_4$ Nanosheet Scaffolds to Promote Photocatalytic Activity in CO_2 Reduction into Methane. *ACS Appl. Mater. Interfaces* **2014**, *6*, 2356–2361.
14. Alotaibi, B.; Fan, S.; Wang, D.; Ye, J.; Mi, Z. Wafer-Level Artificial Photosynthesis for CO_2 Reduction into CH_4 and CO Using GaN Nanowires. *ACS Catal.* **2015**, *5*, 5342–5348.
15. Park, H. A.; Choi, J. H.; Choi, K. M.; Lee, D. K.; Kang, J. K. Highly Porous Gallium Oxide with a High CO_2 Affinity for the Photocatalytic Conversion of Carbon Dioxide into Methane. *J. Mater. Chem.* **2012**, *22*, 5304–5307.
16. Yoshida, M.; Yamakata, A.; Takanabe, K.; Kubota, J.; Osawa, M.; Domen, K. ATR-SEIRAS Investigation of the Fermi Level of Pt Cocatalyst on a GaN Photocatalyst for Hydrogen Evolution under Irradiation. *J. Am. Chem. Soc.* **2009**, *131*, 13218–13219.
17. Pan, Y. X.; Sun, Z. Q.; Cong, H. P.; Men, Y. L.; Xin, S.; Song, J.; Yu, S. H. Photocatalytic CO_2 Reduction Highly Enhanced by Oxygen Vacancies on Pt-Nanoparticle-Dispersed Gallium Oxide. *Nano Res.* **2016**, *9*, 1689–1700.
18. Cao, S.; Zhou, N.; Gao, F.; Chen, H.; Jiang, F. All-Solid-State Z-Scheme 3,4-Dihydroxybenzaldehyde-Functionalized Ga_2O_3/Graphitic Carbon Nitride Photocatalyst with Aromatic Rings as Electron Mediators for Visible-Light Photocatalytic Nitrogen Fixation. *Appl. Catal. B Environ.* **2017**, *218*, 600–610.
19. Li, D.; Kassymova, M.; Cai, X.; Zang, S. Q.; Jiang, H. L. Photocatalytic CO_2 Reduction over Metal-Organic Framework-Based Materials. *Coord. Chem. Rev.* **2020**, *412*, 213262.
20. Dhakshinamoorthy, A.; Li, Z.; Garcia, H. Catalysis and Photocatalysis by Metal Organic Frameworks. *Chem. Soc. Rev.* **2018**, *47*, 8134–8172.
21. Ding, M.; Flaig, R. W.; Jiang, H. L.; Yaghi, O. M. Carbon Capture and Conversion Using Metal-Organic Frameworks and MOF-Based Materials. *Chem. Soc. Rev.* **2019**, *48*, 2783–2828.
22. Dhakshinamoorthy, A.; Asiri, A. M.; García, H. Metal–Organic Framework (MOF) Compounds: Photocatalysts for Redox Reactions and Solar Fuel Production. *Angew. Chem. Int. Ed.* **2016**, *55*, 5414–5445.
23. Fu, Y.; Sun, D.; Chen, Y.; Huang, R.; Ding, Z.; Fu, X.; Li, Z. An Amine-Functionalized Titanium Metal–Organic Framework Photocatalyst with Visible-Light-Induced Activity for CO_2 Reduction. *Angew. Chemie. Int. Ed.* **2012**, *51*, 3364–3367.
24. Lee, Y.; Kim, S.; Kang, J. K.; Cohen, S. M. Photocatalytic CO_2 Reduction by a Mixed Metal (Zr/Ti), Mixed Ligand Metal–Organic Framework Under Visible Light Irradiation. *Chem. Commun.* **2015**, *51*, 5735–5738.
25. Krap, C. P.; Newby, R.; Dhakshinamoorthy, A.; García, H.; Cebula, I.; Easun, T. L.; Savage, M.; Eyley, J. E.; Gao, S.; Blake, A. J.; Lewis, W.; Beton, P. H.; Warren, M. R.; Allan, D. R.; Frogley, M. D.; Tang, C. C.; Cinque, G.; Yang, S.; Schröder, M. Enhancement of CO_2 Adsorption and Catalytic Properties by Fe-Doping of $[Ga_2(OH)_2(L)]$ (H_4L = Biphenyl-3,3′,5,5′-tetracarboxylic Acid), MFM-300(Ga_2). *Inorg. Chem.* **2016**, *55*, 1076–1088.
26. Ma, Z. L.; Wentz, K. M.; Hammann, B. A.; Chang, I.; Kamunde-devonish, M. K.; Cheong, P. H.; Johnson, D. W.; Terskikh, V. V.; Hayes, S. E. Solid-State ^{69}Ga and ^{71}Ga NMR Study of the Nanoscale Inorganic Cluster $[Ga_{13}(\mu_3\text{-}OH)_6(\mu_2\text{-}OH)_{18}(H_2O)_{24}](NO_3)_{15}$. *Chem. Mater.* **2014**, *26*, 4978–4983.

DOI: 10.31635/ccschem.022.202201931
Citation: *CCS Chem.* **2022**, 4, 2560–2569
Link to VoR: https://doi.org/10.31635/ccschem.022.202201931

27. Ling, S.; Slater, B. Unusually Large Band Gap Changes in Breathing Metal–Organic Framework Materials. *J. Phys. Chem. C* **2015**, *119*, 16667–16677.
28. Hou, Y.; Wu, L.; Wang, X.; Ding, Z.; Li, Z.; Fu, X. Photocatalytic Performance of α-, β-, and γ-Ga_2O_3 for the Destruction of Volatile Aromatic Pollutants in Air. *J. Catal.* **2007**, *250*, 12–18.
29. Zeng, J.; Wang, X.; Xie, B.; Li, Q.; Zhang, X. Large π-Conjugated Metal–Organic Frameworks for Infrared-Light-Driven CO_2 Reduction. *J. Am. Chem. Soc.* **2022**, *144*, 1218–1231.
30. Liao, W. M.; Zhang, J. H.; Wang, Z.; Lu, Y. L.; Yin, S. Y.; Wang, H. P.; Fan, Y. N.; Pan, M.; Su, C. Y. Semiconductive Amine-Functionalized Co(II)-MOF for Visible-Light-Driven Hydrogen Evolution and CO_2 Reduction. *Inorg. Chem.* **2018**, *57*, 11436–11442.
31. Wang, D.; Huang, R.; Liu, W.; Sun, D.; Li, Z. Fe-Based MOFs for Photocatalytic CO_2 Reduction: Role of Coordination Unsaturated Sites and Dual Excitation Pathways. *ACS Catal.* **2014**, *4*, 4254–4260.
32. Li, N.; Liu, J.; Liu, J. J.; Dong, L. Z.; Xin, Z. F.; Teng, Y. L.; Lan, Y. Q. Adenine Components in Biomimetic Metal–Organic Frameworks for Efficient CO_2 Photoconversion. *Angew. Chem. Int. Ed.* **2019**, *58*, 5226–5285.
33. Wang, Y. J.; Wang, H. J.; Luo, F.; Yao, S.; Lu, T. B.; Zhang, Z. M. Inter-Clusters Synergy in Iron-Organic Frameworks for Efficient CO_2 Photoreduction. *Appl. Catal. B Environ.* **2022**, *300*, 120487.
34. Qiu, Y. C.; Yuan, S.; Li, X. X.; Du, D. Y.; Wang, C.; Qin, J. S.; Drake, H. F.; Lan, Y. Q.; Jiang, L.; Zhou, H. C. Face-Sharing Archimedean Solids Stacking for the Construction of Mixed-Ligand Metal–Organic Frameworks. *J. Am. Chem. Soc.* **2019**, *141*, 13841–13848.
35. Li, L.; Zhang, S.; Xu, L.; Wang, J.; Shi, L. X.; Chen, Z. N.; Hong, M.; Luo, J. Effective Visible-Light Driven CO_2 Photoreduction via a Promising Bifunctional Iridium Coordination Polymer. *Chem. Sci.* **2014**, *5*, 3808–3813.
36. Yan, Z. H.; Du, M. H.; Liu, J.; Jin, S.; Wang, C.; Zhuang, G. L.; Kong, X. J.; Long, L. S.; Zheng, L. S. Photo-Generated Dinuclear $\{Eu(II)\}_2$ Active Sites for Selective CO_2 Reduction in a Photosensitizing Metal-Organic Framework. *Nat. Commun.* **2018**, *9*, 3353.
37. Zhang, S.; Li, L.; Zhao, S.; Sun, Z.; Luo, J. Construction of Interpenetrated Ruthenium Metal–Organic Frameworks as Stable Photocatalysts for CO_2 Reduction. *Inorg. Chem.* **2015**, *54*, 8375–8379.
38. Xu, H. Q.; Hu, J.; Wang, D.; Li, Z.; Zhang, Q.; Luo, Y.; Yu, S. H.; Jiang, H. L. Visible-Light Photoreduction of CO_2 in a Metal–Organic Framework: Boosting Electron–Hole Separation via Electron Trap States. *J. Am. Chem. Soc.* **2015**, *137*, 13440–13443.
39. Chen, D.; Xing, H.; Wang, C.; Su, Z. Highly Efficient Visible-Light-Driven CO_2 Reduction to Formate by a New Anthracene-Based Zirconium MOF via Dual Catalytic Routes. *J. Mater. Chem. A* **2016**, *4*, 2657–2662.
40. Qin, J. S.; Yuan, S.; Zhang, L.; Li, B.; Du, D. Y.; Huang, N.; Guan, W.; Drake, H. F.; Pang, J.; Lan, Y. Q.; Alsalme, A.; Zhou, H. C. Creating Well-Defined Hexabenzocoronene in Zirconium Metal–Organic Framework by Postsynthetic Annulation. *J. Am. Chem. Soc.* **2019**, *141*, 2054–2060.
41. Sun, M.; Yan, S.; Sun, Y.; Yang, X.; Guo, Z.; Du, J.; Chen, D.; Chen, P.; Xing, H. Enhancement of Visible-Light-Driven CO_2 Reduction Performance Using an Amine-Functionalized Zirconium Metal–Organic Framework. *Dalton. Trans.* **2018**, *47*, 909–915.
42. Dong, L.; Zhang, L.; Liu, J.; Huang, Q.; Lu, M.; Ji, W.; Lan, Y. Stable Heterometallic Cluster-Based Organic Framework Catalysts for Artificial Photosynthesis. *Angew. Chem. Int. Ed.* **2020**, *59*, 2659–2663.
43. Sun, D.; Liu, W.; Qiu, M.; Zhang, Y.; Li, Z. Introduction of a Mediator for Enhancing Photocatalytic Performance via Post-Synthetic Metal Exchange in Metal–Organic Frameworks (MOFs). *Chem. Commun.* **2015**, *51*, 2056–2059.
44. Sun, D.; Fu, Y.; Liu, W.; Ye, L.; Wang, D.; Yang, L.; Fu, X.; Li, Z. Studies on Photocatalytic CO_2 Reduction over NH_2-Uio-66 (Zr) and Its Derivatives: Towards a Better Understanding of Photocatalysis on Metal-Organic Frameworks. *Chem. A Eur. J.* **2013**, *19*, 14279–14285.
45. Wang, C.; Xie, Z.; Dekrafft, K. E.; Lin, W. Doping Metal-Organic Frameworks for Water Oxidation, Carbon Dioxide Reduction, and Organic Photocatalysis. *J. Am. Chem. Soc.* **2011**, *133*, 13445–13454.
46. Morimoto, T.; Nakajima, T.; Sawa, S.; Nakanishi, R.; Imori, D.; Ishitani, O. CO_2 Capture by a Rhenium(I) Complex with the Aid of Triethanolamine. *J. Am. Chem. Soc.* **2013**, *135*, 16825–16828.
47. Sampaio, R. N.; Grills, D. C.; Polyansky, D. E.; Szalda, D. J.; Fujita, E. Unexpected Roles of Triethanolamine in the Photochemical Reduction of CO_2 to Formate by Ruthenium Complexes. *J. Am. Chem. Soc.* **2020**, *142*, 2413–2428.
48. Volkringer, C.; Loiseau, T.; Guillou, N.; Férey, G.; Elkaïm, E.; Vimont, A. XRD and IR Structural Investigations of a Particular Breathing Effect in the MOF-Type Gallium Terephthalate MIL-53(Ga). *Dalton. Trans.* **2009**, *53*, 2241–2249.
49. Wieme, J.; Lejaeghere, K.; Kresse, G.; Van Speybroeck, V. Tuning the Balance Between Dispersion and Entropy to Design Temperature-Responsive Flexible Metal-Organic Frameworks. *Nat. Commun.* **2018**, *9*, 4899.
50. Christophe, V.; Meddouri, M.; Loiseau, T.; Guillou, N.; Marrot, J.; Fe´rey, G.; Haouas, M.; Taulelle, F.; Audebrand, N.; Latroche, M. The Kagomé Topology of the Gallium and Indium Metal-Organic Framework Types with a MIL-68 Structure: Synthesis, XRD, Solid-State NMR Characterizations, and Hydrogen Adsorption. *Inorg. Chem.* **2008**, *47*, 11892–11901.
51. Zhang, R.; Song, X.; Liu, Y.; Wang, P.; Wang, Z.; Zheng, Z.; Dai, Y.; Huang, B. Monomolecular VB_2-Doped MOFs for Photocatalytic Oxidation with Enhanced Stability, Recyclability and Selectivity. *J. Mater. Chem. A* **2019**, *7*, 26934–26943.
52. Guo, S. H.; Guo, S. H.; Qi, X. J.; Zhou, H. M.; Zhou, J.; Wang, X. H.; Dong, M.; Zhao, X.; Sun, C. Y.; Wang, X. L.; Su, Z. M.; Su, Z. M. A Bimetallic-MOF Catalyst for Efficient CO_2 Photoreduction from Simulated Flue Gas to Value- Added Formate. *J. Mater. Chem. A* **2020**, *8*, 11712–11718.
53. Buettner, G. R. Spin Trapping: ESR Parameters of Spin Adducts 1474 1528V. *Free Radic. Bio. Med.* **1987**, *3*, 259–303.

DOI: 10.31635/ccschem.022.202201931
Citation: *CCS Chem.* **2022**, 4, 2560–2569
Link to VoR: https://doi.org/10.31635/ccschem.022.202201931

54. Walger, E.; Marlin, N.; Mortha, G.; Molton, F.; Duboc, C. Hydroxyl Radical Generation by the H_2O_2/Cu^{II}/Phenanthroline System under Both Neutral and Alkaline Conditions: An EPR/Spin-Trapping Investigation. *Appl. Sci.* **2021**, *11*, 687.
55. Gimat, A.; Kasneryk, V.; Dupont, A. L.; Paris, S.; Averseng, F.; Fournier, J.; Massiani, P.; Rouchon, V. Investigating the DMPO-Formate Spin Trapping Method for the Study of Paper Iron Gall Ink Corrosion. *New J. Chem.* **2016**, *40*, 9098–9110.
56. Habisreutinger, S. N.; Schmidt-Mende, L.; Stolarczyk, J. K. Photocatalytic Reduction of CO_2 on TiO_2 and Other Semiconductors. *Angew. Chem. Int. Ed.* **2013**, *52*, 7372–7408.
57. Takezawa, H.; Shitozawa, K.; Fujita, M. Enhanced Reactivity of Twisted Amides Inside a Molecular Cage. *Nat. Chem.* **2020**, *12*, 574–578.
58. Lin, L.; Sheveleva, A. M.; Silva, D.; Parlett, I. C.; Tang, Z.; Liu, Y.; Fan, M.; Han, X.; Carter, J. H.; Tuna, F.; McInnes, E. J. L.; Cheng, Y.; Daemen, L. L.; Rudić, S.; Ramirez-Cuesta, A. J.; Tang, C. C.; Yang, S. Quantitative Production of Butenes from Biomass-Derived γ-Valerolactone Catalysed by Hetero-Atomic MFI Zeolite. *Nat. Mater.* **2020**, *19*, 86–93.

DOI: 10.31635/ccschem.022.202201931
Citation: *CCS Chem.* **2022**, 4, 2560–2569
Link to VoR: https://doi.org/10.31635/ccschem.022.202201931